Earth and Planetary Science Letters 457 (2017) 10–22

Contents lists available at ScienceDirect

Earth and Planetary Science Letters

www.elsevier.com/locate/epsl

Propagating buoyant mantle upwelling on the Reykjanes Ridge

Fernando Martinez *, Richard Hey

Hawaii Institute of Geophysics and Planetology, School of Ocean and Earth Science and Technology, University of Hawaii at Manoa, Honolulu, HI 96822, USA

ARTICLE INFO

Article history:
Received 24 February 2016
Received in revised form 22 June 2016
Accepted 15 September 2016
Available online 21 October 2016
Editor: C. Sotin

Keywords:
plate boundary processes
mid-ocean ridges
mantle plumes

ABSTRACT

Crustal features of the Reykjanes Ridge have been attributed to mantle plume flow radiating outward from the Iceland hotspot. This model requires very rapid mantle upwelling and a "rheological boundary" at the solidus to deflect plume material laterally and prevent extreme melting above the plume stem. Here we propose an alternative explanation in which shallow buoyant mantle upwelling instabilities propagate along axis to form the crustal features of the ridge and flanks. As only the locus of buoyant upwelling propagates this mechanism removes the need for rapid mantle plume flow. Based on new geophysical mapping we show that a persistent sub-axial low viscosity channel supporting buoyant mantle upwelling can explain the current oblique geometry of the ridge as a reestablishment of its original configuration following an abrupt change in opening direction. This mechanism further explains the replacement of ridge-orthogonal crustal segmentation with V-shaped crustal ridges and troughs. Our findings indicate that crustal features of the Reykjanes Ridge and flanks are formed by shallow buoyant mantle instabilities, fundamentally like at other slow spreading ridges, and need not reflect deep mantle plume flow.

1. Introduction

The Iceland hotspot has long been viewed as formed by a mantle plume (Morgan, 1971) and as the Reykjanes Ridge intersects this feature its axial and flanking tectonic and crustal characteristics have been assumed to reflect mantle plume flow and temperature (Vogt, 1971). As proposed in conceptual models by Vogt (1971), thermal pulses rapidly rise within a plume stem beneath Iceland and then either spread radially or are channeled along-axis to form V-shaped crustal ridges as they flow beneath the Reykjanes Ridge. The geometry of the V-shaped ridges implies that mantle plume flow is at least ten times the spreading rate (Vogt, 1971). Of Vogt's two alternative flow models, current geodynamic models favor radial pancake-like expansion of the plume head that implies even faster upwelling in the plume stem as a result of radial spreading. Ito (2001) recognized that rapidly upwelling thermal pulses in the mantle plume stem would generate extreme crustal thickness variations (>200 km) if allowed to melt by decompression. To avoid these unobserved crustal thicknesses he proposed that a high viscosity "rheological boundary" formed by mantle dehydration (Hirth and Kohlstedt, 1996) above the solidus laterally deflects the plume before it melts (Ito, 2001). Because of the high viscosities above the solidus required in this model, ridge melting regime flow is purely plate-driven "corner flow" and only the component of upwelling required by passive plate spreading draws plume material into the sub-axial melting regime. In this model there is no sub-axial channeled plume flow and the V-shaped crustal ridges are generated as solid state plume material with embedded thermal pulses expands radially in annular rings beneath the high viscosity dehydration layer and solidus and are locally advected by ridge spreading. Thus excess crustal thicknesses beneath Iceland and the V-shaped ridges are generated thermally (not by enhanced upwelling) by a small component of plume material that is advected by passive plate spreading above the solidus into the high viscosity dehydration layer where it can melt by decompression. Mantle flow above the solidus has only corner flow trajectories (vertical beneath the axis curving to horizontal and spreading direction-parallel on the flanks) with no along-axis components and is radial beneath the solidus and high viscosity layer and centered beneath Iceland. We refer to this model hereafter as the pulsing plume model, as described by Ito (2001).

The pulsing plume model contrasts in fundamental ways with current models of slow spreading mid-ocean ridges wherein low mantle viscosity and buoyant upwelling instabilities are thought to be important in sub-axial mantle flow (Forsyth, 1992). In these models cells of buoyant mantle upwelling account for the segmented and focused nature of crustal accretion at slow spreading ridges. The buoyant upwelling cells generate crustal thickness variations from their centers to their ends forming fracture zones (FZs) or non-transform discontinuities (NTDs) whether or not ridge seg-

* Corresponding author.
E-mail address: fernando@hawaii.edu (F. Martinez).

http://dx.doi.org/10.1016/j.epsl.2016.09.057
0012-821X/

ments are offset (Tucholke et al., 1997). The significant contribution of buoyant upwelling to melting distinguishes slow spreading ridges from fast spreading ridges where two-dimensional plate-driven "passive" mantle upwelling dominates and crustal segmentation can only occur at ridge segment offsets (Phipps Morgan and Forsyth, 1988). In the North Atlantic slow spreading (~20 mm/yr, total rate) and regionally enhanced mantle melting should especially favor buoyant mantle upwelling. However, these general features of slow spreading ridges are precluded by the requirement of a high viscosity boundary layer in pulsing plume models. Together with other anomalous features, such as its 30° oblique spreading, linear geometry, and apparent lack of crustal segmentation, the Reykjanes Ridge presents a seeming contradiction to general models of slow spreading ridges. To examine these issues, we conducted a detailed marine geophysical survey of the southern Reykjanes Ridge and interpreted the results in the context of North Atlantic regional tectonics. We find that the reconfiguration of the ridge, elimination of segmentation, its present oblique linear geometry and formation of flanking crustal V-shaped ridges can be consistently explained by upper mantle buoyant upwelling, if such instabilities can propagate along a long linear axis.

1.1. Geologic background

Early seafloor spreading in the North Atlantic basin was partitioned between dual spreading centers. The Ran Ridge in the Labrador Sea between Greenland and North America initiated around 60 Ma (Vogt and Avery, 1974). The proto Reykjanes Ridge between Greenland and Eurasia initiated around 55 Ma (Vogt and Avery, 1974). These spreading centers joined the southward continuation of the Mid-Atlantic Ridge at a triple junction near what later became the Bight Fracture Zone. The proto Reykjanes Ridge formed an orthogonally spreading linear ridge without major offsets or FZs (Smallwood and White, 2002), as shown by the pattern of magnetic (Macnab et al., 1995) and gravity (Sandwell et al., 2014) anomalies in regional compilations (Fig. 1). Near Anomaly 17 (~37 Ma) the opening direction abruptly changed by ~30° from NW–SE to nearly E–W (Smallwood and White, 2002), probably related to cessation of spreading in the Labrador Sea and joining of Greenland to the North American plate (Vogt and Avery, 1974). This tectonic reconfiguration also converted the North America–Greenland–Eurasia triple junction into the Bight transform fault. As a result of the change in opening direction the Reykjanes Ridge abruptly became fragmented (Smallwood and White, 2002) forming a ridge-transform stair-step pattern with ~50 km long ridges offset by transform faults on the order of 30 km long. Immediately after this segmented plate boundary was established it began to reconfigure again, but this time diachronously from north to south, so that a single linear but now obliquely spreading ridge replaced the orthogonally-spreading stair-step geometry (Hey et al., 2016). This reconfiguration occurred without further significant changes in opening direction (Smallwood and White, 2002) and was accompanied by the formation of diachronous V-shaped crustal ridges and troughs (Vogt, 1971), and the elimination of the previous ridge-orthogonal crustal segment offsets and boundaries (Fig. 1B).

1.2. Survey objectives

In order to investigate the elimination of transform faults, FZs and NTDs, the change from orthogonal to oblique spreading and the formation of V-shaped crustal ridges and troughs we surveyed the Reykjanes Ridge and flanks near its intersection with the Bight Transform Fault in August–September 2013 on *R/V Marcus G. Langseth*. In this area FZs and a transform fault still approach and intersect the ridge axis so that the process that eliminated them can be most clearly examined. Basement structure is well imaged in multibeam sonar mapping and closely spaced gravity and magnetic profiles resolve three-dimensional variations reflecting crustal thickness and deeper mantle density variations and magnetic isochrons. The magnetic isochrons together with seafloor basement fabric map the evolution of the plate boundary in sufficient detail to show how it reconfigured thereby allowing tests of proposed mantle plume-induced "thermal weakening" models (Vogt and Johnson, 1975; White, 1997) involving gradual ridge rotation vs. tectonic ridge propagation (Hey, 1977) and other ridge migration processes by asymmetric spreading. Mantle Bouguer anomalies map out changes in crustal thickness and underlying mantle density structure between the orthogonal segment south of the Bight FZ and the developing oblique ridge segments to the north providing insights into how the mode of mantle advection changed between these settings.

2. Methods

2.1. Multibeam data processing

Bathymetry and acoustic backscatter data were acquired with a 1° × 1° Simrad EM122 multibeam system on *R/V Marcus G. Langseth*. The multibeam system was calibrated daily with expendable bathy thermograph (XBT) water column sound velocity profiles. Tracks were run along flowlines calculated from Smallwood and White (2002) rotation poles for North America–Eurasia and mostly spaced at 7 km. The bathymetric data were gridded in .001 × .001 degree cells in latitude and longitude using Generic Mapping Tools (GMT) (Wessel et al., 2013) and MB-System (Caress and Chayes, 2008) software. The gridded bathymetric surface was illuminated from 045° and is shown with depths color coded in Fig. 2A. Acoustic backscatter data were extracted from the multibeam files and gridded at .0005 × .00025 degree cells in longitude and latitude. The acoustic backscatter data are shown in Fig. 2B as a gray-scale map with higher values in darker shades. The gridded multibeam data provide essentially complete coverage between tracks.

2.2. Magnetics data processing

Magnetic field data were acquired with a Geometrics G-882 Cesium magnetometer towed 200 m behind the ship during essentially all of the survey. The International Geomagnetic Reference Field (IGRF) was removed from the total field values to produce magnetic anomalies and gridded using GMT software. Extrapolated grid values were masked to the approximate extent of the multibeam data and plotted as a color-coded map in Fig. 3A. Isochrons (Fig. 3A) were identified from observed profile values by comparison with forward calculated two-dimensional magnetic profiles generated by block models of the geomagnetic reversal sequence scaled for the half-spreading rate of the Reykjanes Ridge (11 mm/yr) in Mirone Software (Luis, 2007). Three-dimensional magnetic anomaly and bathymetry grids were used to calculate seafloor magnetization, which removes field skewness and topographic effects. The magnetization inversion used magnetic grid (Macnab et al., 1995) and ship (Searle et al., 1998) and satellite-predicted (Sandwell et al., 2014) bathymetry to fill in areas outside of our survey coverage (gray areas in Fig. 3A). The grids were resampled to approximately 1 km spacings and mirrored for the magnetization inversion to minimize edge effects. The inversion used a three-dimensional implementation (Luis, 2007) of the Parker (1972) method in the Fourier domain. A 500 m source layer was assumed with magnetization direction given by an axial geocentric dipole. Five terms in the Fourier series were used. Data values were masked to the extent of the *Langseth* multibeam grid and are shown with color-coded values in Fig. 3B. As the resulting

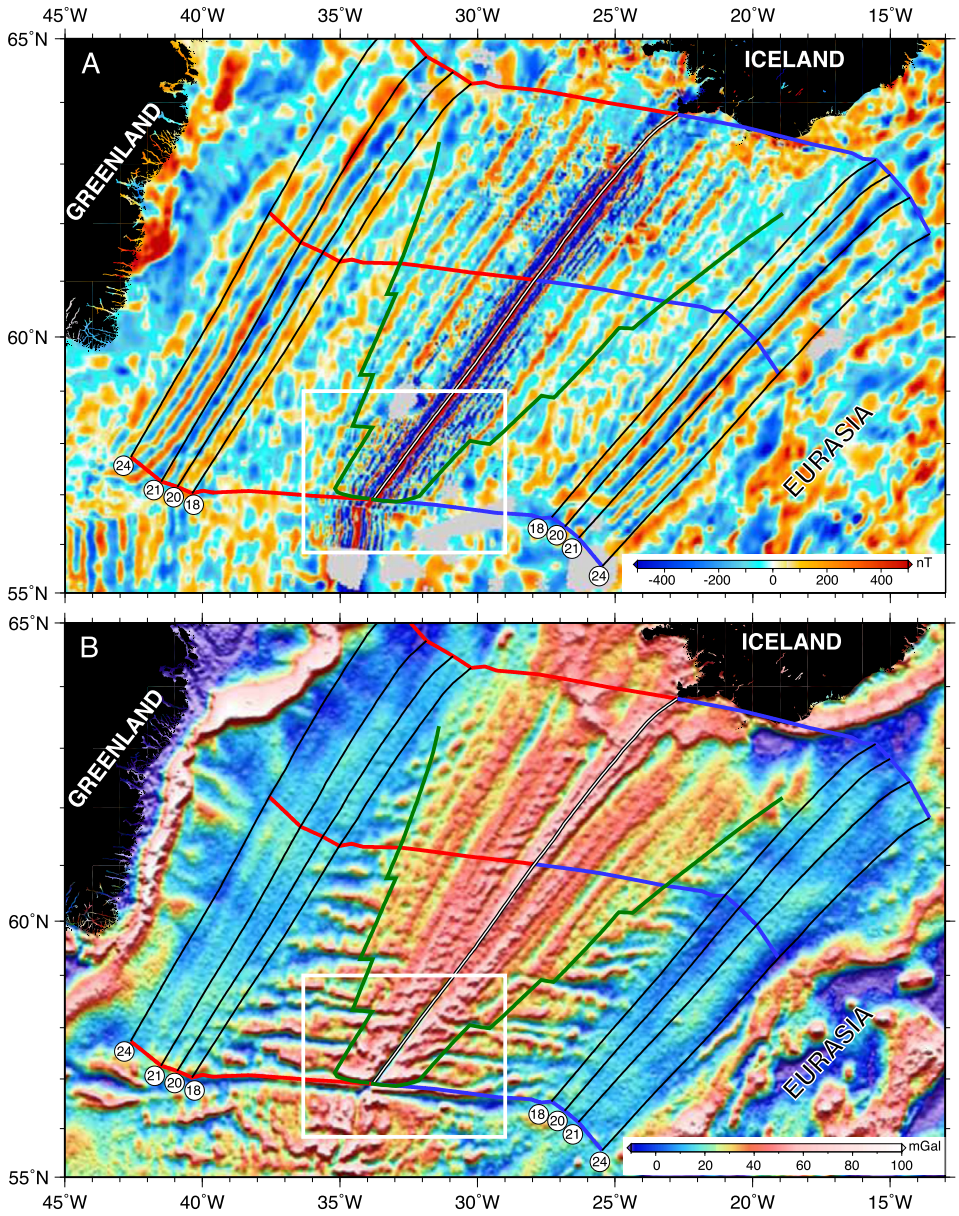

Fig. 1. (A) Regional compiled magnetic anomaly grid (Macnab et al., 1995) with R/V Langseth (MGL1309), RRS Charles Darwin (CD87) (Searle et al., 1998) and R/V Knorr (KN189-4) (Hey et al., 2010) ship data added. (B) Satellite-derived free air gravity anomaly (Sandwell et al., 2014). Fine double line marks the current Reykjanes Ridge axis. Black lines show the reconstructed position of the current ridge axis rotated according to the Greenland–Eurasia finite rotation poles for Anomalies 18, 20, 21, and 24 (labeled circles) of Smallwood and White (2002). The red and blue lines are flow lines calculated according to their stage poles to the present day for the Greenland and Eurasian plates respectively and trace the opening directions through time. White outlined box indicates survey area shown in Figs. 2–4. Near Anomaly 17 time (~37 Ma) (adjacent to young side of labeled Anomaly 18) the direction of opening changed by about 30° and the plate boundary abruptly became segmented and offset as shown by offset magnetic lineations (A) and the initiation of prominent fracture zone troughs (B). Green line broadly indicates the subsequent reconfiguration boundary between segmented and unsegmented crust that developed diachronously and without further significant changes in opening direction (Smallwood and White, 2002). When the ridge axis became segmented near Anomaly 17 time the new ridge segments were spreading orthogonally to the new opening direction as shown by the parallel orientation of the fracture zone troughs and flow lines (B). Subsequently the plate boundary reconfigured diachronously from north to south. Offset segments merged back to their original linear configuration over the mantle as shown by the parallel geometry of the rotated axis (black lines) and the early-formed magnetic anomaly lineations, despite the current axis now being ~30° oblique to the opening direction and the intervening stair-step fragmentation of the plate boundary (A).

magnetization map (Fig. 3B) agreed in polarity transitions with the total field anomaly map (Fig. 3A) no annihilator (Parker, 1972) was added.

2.3. Gravity data processing

Gravity data were acquired at 1-second intervals with a Bell BGM-3 gravimeter mounted on a gyro-stabilized platform. A running 10-minute cosine taper was applied and data output at 10-second intervals. Eotvos corrections for ship speed, course, and latitude were applied. The International Gravity Formula correction using WGS84 ellipsoid parameters was removed to yield the free air gravity anomaly. Comparison of *Langseth* and satellite-derived free-air gravity data (Sandwell et al., 2014) and gravity tie values at the start and end of the cruise (both at Reykjavik) showed no systematic drift. The free air anomaly values were gridded using GMT software, masked to the extent of the multibeam data, and are shown as a color-coded map with 10 mGal contours in Fig. 4A.

Three-dimensional mantle Bouguer anomaly (MBA) values were calculated following the method of Kuo and Forsyth (1988). We used satellite predicted values and *RRS Charles Darwin* multibeam data (Searle et al., 1998) to fill in gaps outside of the *Langseth*

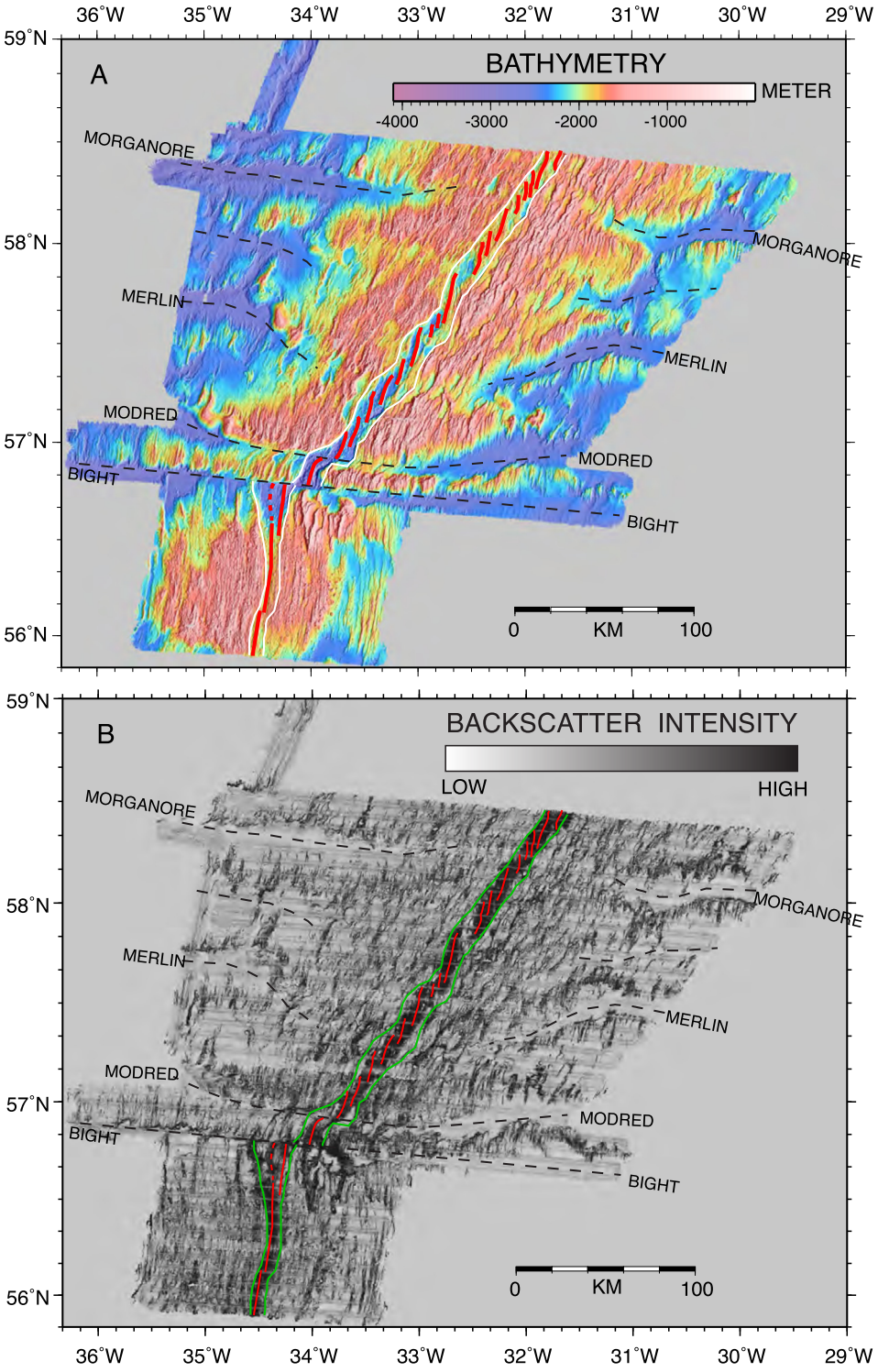

Fig. 2. Multibeam data from *R/V Marcus G. Langseth* survey. Fracture zone and non-transform discontinuities are labeled and shown as dashed lines. A) Multibeam bathymetry showing axial volcanic ridges (red lines) and interpreted limit of the plate boundary zone (white line). B) Acoustic backscatter imagery showing axial volcanic ridges (red lines) and plate boundary zone (green line). The labeled Bight FZ has been stable since after about anomaly 17 (~37 Ma) and gives the plate opening direction for the local surveys (Figs 2–4). See Methods section for details on data processing.

multibeam data coverage. Because of spatial distortion at high latitudes, the bathymetry data were converted from geographic coordinates to projected meters using a transverse Mercator projection with a central meridian at 33°W. The projected data were gridded at about 550 m spacing producing a 1024×1024 cell grid. This grid was then mirrored to reduce edge effects and used to forward calculate the gravity effect of the seafloor and Moho assuming a 6 km thick crust and density contrast of 1670 kg/m^3 at the seafloor and 600 kg/m^3 at the Moho. Five terms in the Fourier series were used. The forward calculated gravity grids were inverse transformed to geographic coordinates and subtracted from each free air anomaly value to yield the MBA. The MBA values were then gridded using GMT software, masked to the extent of the multibeam data, and are shown as a color-coded map with 5 mGal contours in Fig. 4B.

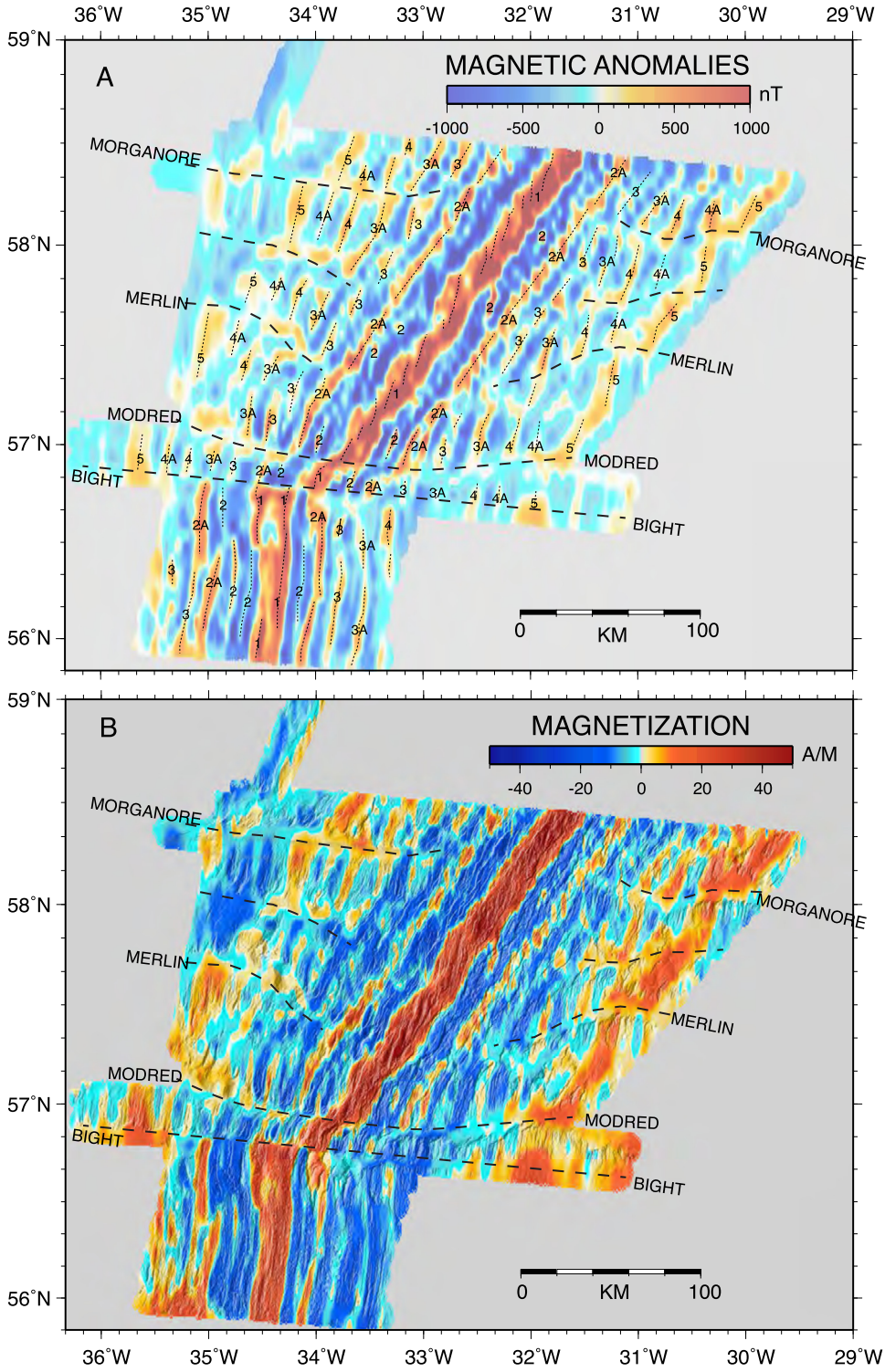

Fig. 3. Magnetics data from *R/V Marcus G. Langseth* survey. A) Magnetic anomalies and isochrons (labeled fine dotted lines). B) Seafloor magnetization inversion. See Methods section for details on data processing.

3. Results

3.1. Basement structure

Vogt and Avery (1974) named the main FZs flanking the Reykjanes Ridge and we follow their convention here. In the surveyed area, the spreading center forms a 10–15 km wide valley surrounding axial volcanic ridges which, north of the Bight transform fault, are arrayed en echelon (Searle et al., 1998). Seafloor backscatter data derived from the EM122 multibeam system (Fig. 2B) delineate the neo-volcanic zone as a high amplitude band generally confined to the axial valley. The axial valley and nearly co-extensive neo-volcanic zone correspond to a "plate boundary zone" where active tectonic deformation and volcanism occur and where most of the crust is accreted before the lithosphere becomes part of stronger flanking and essentially non-internally deforming "rigid" plates (Macdonald, 1982). The limit of the plate boundary zone is interpreted to lie just beyond

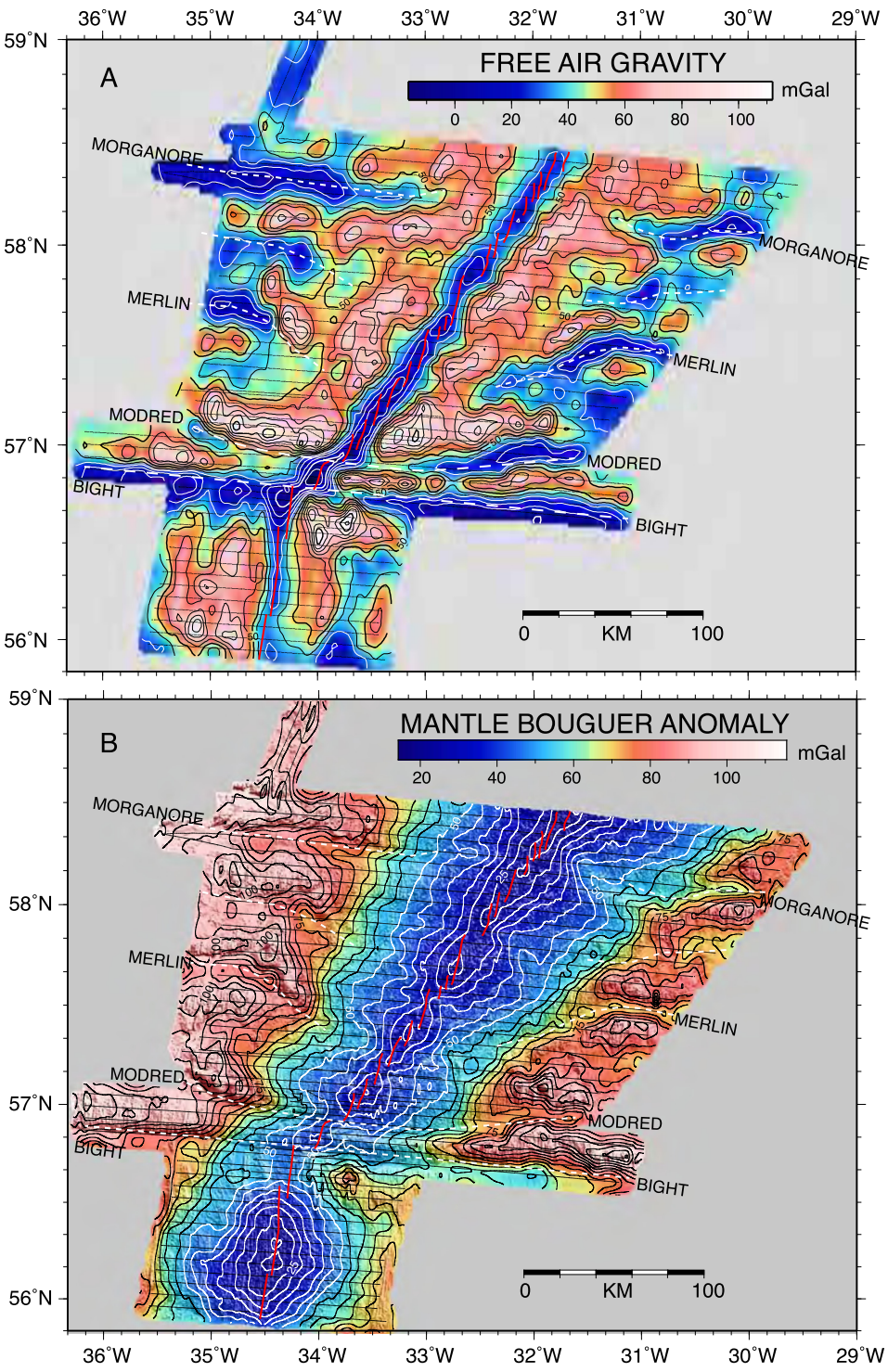

Fig. 4. Gravity data from *R/V Marcus G. Langseth* survey. A) Free air gravity anomalies with 10 mGal contours. B) Mantle Bouguer gravity anomalies with 5 mGal contours. See Methods section for details on data processing.

the upper edge of the axial valley and is indicated in Figs. 2A and B.

Axial and ridge flank structures are determined by a combination of volcanic and tectonic processes. Within the neovolcanic zone, axial volcanic ridges (AVRs) are generally linear with an orientation approximately orthogonal to the opening direction whether the overall plate boundary zone is orthogonal or oblique. As spreading-orthogonal axial volcanic ridges are translated outward, they become tectonized (Parson et al., 1993) and dissected by major faulting within the plate boundary zone and axial valley walls. Thus different ridge flank basement fabric develops depending on whether the spreading-orthogonal AVRs have been dissected by an orthogonal or oblique plate boundary zone and axial valley.

Regional gravity maps (Fig. 1) and our detailed survey (Fig. 2A) indicate that some FZs deviate from calculated flow lines but depart more strongly closer to the current axis. This suggests increasing instability of the segmentation boundaries with time, changing from flowline parallel FZs to NTDs that migrate along axis. Where FZs and NTDs are well developed (Figs. 2A and B) ridge flank crust

has primarily spreading-orthogonal fabric. As these discontinuities disappear approaching the axis, seafloor fabric acquires a more complex orthogonal and oblique fabric. This broad trend suggests that while FZs and NTDs are present the plate boundary zone is orthogonal to the spreading direction and as these boundaries are eliminated the plate boundary zone becomes oblique.

The Bight FZ appears to have formed from a true transform fault since its inception when the Labrador Sea spreading center failed and eliminated a previous triple junction (Vogt and Avery, 1974). The orthogonal spreading segment south of the Bight FZ has seafloor fabric that is primarily orthogonal to the spreading direction. The current axis displays several third-order segment offsets (Figs. 2A and B). At the northern end of the orthogonal segment the axis appears to have jumped eastward within the Brunhes anomaly (Benediktsdóttir et al., 2016). The sense of ridge jumps shortens the offset length with the ridge segment to the north across the Bight transform fault.

3.2. Magnetic isochrons and seafloor magnetization

Isochron identifications (Fig. 3A) show that older anomalies are approximately orthogonally oriented to the spreading direction and are offset across the major FZs and NTDs whereas younger anomalies become continuous along-axis and oblique. Yet this change does not take place discontinuously, as would occur by the propagation of an unsegmented oblique axis replacing a segmented orthogonal axis. In the survey area north of the Bight FZ there are no clear indications of standard ridge propagation features such as pseudofaults, failed rifts and transferred lithosphere (Hey et al., 1980). Rather, isochron offsets across segment boundaries decrease with time towards younger ages. These observations imply that offset and orthogonally spreading segments migrate towards each other before merging into an oblique axis. For example, Fig. 3A shows that across the western limb of the Merlin FZ Anomaly 5 is offset by over 20 km but by Anomaly 3 the offset is only about 5 km and by Anomaly 2A the offset is virtually eliminated and the isochron is continuous. Accompanying the decrease in ridge offset across segment boundaries is a change in the nature and behavior of the offset. In several cases what appear to have been true transform faults based on their flowline geometry near the outer edges of the survey first become migrating NTDs as segment offsets decrease before these become indistinct as the spreading segments rapidly merge into an oblique axis. In several cases what had been single long anomalies between the major FZs develop offsets in younger anomalies indicating that longer segments break up into smaller segments in order to merge into an oblique linear axis (Fig. 3A and B). This breakup into smaller length spreading segments may occur because the basic units of crustal accretion, the AVRs, remain nearly orthogonal to the spreading direction, yet evolve to an en echelon configuration to accommodate a linear oblique plate boundary zone.

Therefore ridge axes do not rotate into obliquity as proposed by Vogt and Johnson (1975), nor are they replaced by propagating oblique ridges, but rather the ridges first migrate laterally to reduce offsets between segments and then subdivide into smaller en echelon segments until the entire plate boundary zone achieves a continuous, linear and oblique configuration. To the north of our survey a detailed identification of magnetic isochrons over the Neogene and Quaternary (Merkouriev and DeMets, 2014) confirms the general pattern of decreasing segment offsets with time before the establishment of a linear oblique plate boundary configuration.

Within the survey area a pattern of progressive northward merging and alignment of segments to a linear axis is evident in the shape of the Brunhes central anomaly shown in the magnetization map (Fig. 3B). A truncation and step-like offset of the Brunhes positive magnetization band occurs at the Bight FZ. North of the Bight FZ a continuous Brunhes magnetization band is evident across the Modred NTD but forms prominent sinuous deviations from linearity at the discontinuity. Farther north major segmentation discontinuities no longer reach to the axis but a sinuous shape to the Brunhes magnetization band is still evident. At about 58°N the Brunhes magnetization band establishes an essentially linear trend that continues northward (Lee and Searle, 2000).

3.3. Gravity anomalies

The MBA map (Fig. 4B) shows a broad low associated with the spreading axis and higher values associated with the flanks. Note that near the ridge axis segment boundaries form relative MBA highs separating the large “bulls-eye” low south of the Bight FZ and smaller lows to the north. Off axis the pattern is reversed with FZ and NTDs forming relative gravity lows between crustal highs. Assuming that crustal segmentation boundaries that form bathymetric troughs (FZs and NTDs) represent thin crust (Kuo and Forsyth, 1988), the off-axis MBA lows imply low density material along these zones out of isostatic equilibrium. The simplest explanation is that flankward increasing thickness of low-density sediments not accounted for in the MBA reduction accounts for the lows along the FZs and NTDs. Additional factors may include increasing flankward crustal alteration formed when axial offsets were larger as shown by magnetic isochrons (Fig. 3A). Larger offsets may lead to increased tectonization and alteration of crustal and mantle material. As these areas move farther off axis lithospheric cooling may also depress the thermal serpentinization front increasing mantle serpentinization. These combined effects may lead to progressive lowering of density and the observed gravity inversion along FZ and NTD discontinuities.

The MBA low associated with the axis shows different patterns north and south of the Bight FZ. The orthogonally spreading segment south of the Bight FZ displays a large “bulls-eye” low typical of orthogonal slow spreading ridges (Kuo and Forsyth, 1988). The axis north of the Bight FZ displays smaller circular patterns that northward become individually less distinct and merge into a single elongated axial low even as the overall amplitude of the low becomes larger and wider. The change in bathymetry and MBA gravity from a “bulls-eye” low in the orthogonal and transform bound segment south of the Bight FZ to a more uniform along-axis low implies a distinct change in the manner of mantle upwelling and crustal accretion (Kuo and Forsyth, 1988). The overall northward broadening of the axial low roughly follows the boundary between segmented and unsegmented crust.

4. Discussion

4.1. Geodynamic pulsing plume models

Current geodynamic models of the Reykjanes Ridge generally follow the conceptual model of Vogt (1971) and view its flanking V-shaped ridges as direct indicators of mantle plume flow with embedded thermal variations. Under this assumption, estimated flow rates along-axis based on the geometry of the V-shaped ridges range from about 168 mm/yr (Ito, 2001) to over 1000 mm/yr (Wright and Miller, 1996). If these rates represent radial flow, upwelling rates within the plume stem must be even faster due to radial spreading and slowing of the flow. Ito (2001) recognized that such rapid upwelling of hot plume mantle would lead to extreme crustal production above the plume stem through decompression melting and calculated that >200 km crustal thickness variations should be expected from the plume pulses. Most plume melting would occur directly over the stem and largely depleted mantle material would be left over to form the horizontally radially expanding plume “pancake”, which would not form V-shaped

crustal ridges (Ito, 2001). To avoid these problems he proposed that a dehydrated high viscosity rheological boundary forms above the solidus that deflects the mantle plume horizontally before it melts. Only the component of passive mantle upwelling required by slow plate spreading at the Reykjanes Ridge and Iceland would then draw up a small fraction of plume material to melt and form the V-shaped crustal ridges and troughs as the thermal pulses embedded in the plume head expanded radially. The strong rheological boundary is a required part of pulsing plume models forming an essentially flat surface following the solidus at the time of mantle melting so that channeled sub-axial "pipe flow" (Vogt, 1971) and buoyant mantle advection cannot occur within the sub-axial ridge melting regime and the pattern of mantle advection therefore has a passive "corner flow" form (Reid and Jackson, 1981).

A dilemma in the pulsing plume model is that a rheological dehydration boundary capable of deflecting the Iceland plume, suggested by some to be the strongest on Earth today (Parnell-Turner et al., 2014), should preclude all plume volcanism away from a spreading center. A dehydrated rheological boundary should be a general property of all residual oceanic lithosphere formed by mantle melting and dehydration at mid-ocean ridges (Hirth and Kohlstedt, 1996) and by mantle plumes anywhere. Yet intra-plate mantle plumes such as at Hawaii evidently penetrate this boundary producing voluminous volcanism in the absence of a spreading center. This dilemma is exacerbated at Hawaii because the hypothesized strong dehydration rheological boundary should be embedded within an even more viscous thermal boundary layer associated with ∼90 Ma Pacific lithosphere and thus should present an even more impenetrable boundary to the weaker Hawaiian plume. At Hawaii deep melting beneath the thermal lithosphere may explain the hotspot volcanism, yet the pulsing plume model for Iceland precludes this mechanism. At the ridge-centered Iceland plume there is essentially no thermal boundary layer above the plume and only the dehydration layer is invoked to deflect the plume to prevent extreme melting. In the pulsing plume model, mantle melting is attributed solely to plate spreading that draws up only a small component of the total large flux of plume material that in the absence of a spreading center would all flow away horizontally beneath the solidus without melting (Ito, 2001). Following this theory, there should be no melting due to mantle plumes at intra-plate settings such as Hawaii where a thick thermal boundary layer adds to the rheological boundary produced by ubiquitous dehydration of upper oceanic lithosphere.

In contrast, as we show below, a persistent low viscosity sub-axial lithospheric channel or melting regime within which buoyant mantle upwelling can occur is likely to exist beneath the Reykjanes Ridge and Iceland. It can explain the large-scale tectonic reorganizations of the Reykjanes Ridge, its current oblique linear geometry, the removal of ridge-orthogonal crustal segmentation boundaries and the formation of the V-shaped ridges. Our model removes the need for rapid mantle plume upwelling and therefore the need for a rheological boundary to deflect the plume and is consistent with fundamental processes of mantle upwelling, melting and crustal accretion at slow-spreading mid-ocean ridges (Forsyth, 1992).

4.2. Propagating sub-axial buoyant mantle upwelling

Models for the changes in tectonic configuration of the Reykjanes Ridge generally agree that the abrupt change in opening direction around Anomaly 17 triggered the breakup of the linear ridge to a stair-step geometry (Vogt and Avery, 1974). This reconfiguration was therefore likely a mechanical response of the lithosphere to a new stress orientation and not a result of changes in mantle thermal structure or flow. Similar kinematically-driven plate boundary reconfigurations unassociated with hotspots are well documented in the Parece Vela (Okino et al., 1998) and Woodlark basins (Goodliffe et al., 1997). These observations support the hypothesis that abrupt plate boundary reconfigurations at times of plate motion change are lithospheric responses to changing stresses and are not associated with mantle plume effects.

The Reykjanes Ridge stair-step pattern, however, began to reconfigure again from north to south just after forming without further significant changes in opening direction (Smallwood and White, 2002). Most models view this later reconfiguration as a result of regional hot mantle plume material radiating outward, weakening the lithosphere so that it becomes ductile, thus eliminating transform faults and segmentation boundaries (White, 1997). Yet a simple thermal weakening of the lithosphere would likely only convert transform faults to non-transform discontinuities and does not account for the merging of the offset ridge axes to a linear and obliquely spreading ridge. Further, the fact that in the pulsing plume model the dehydration layer is not thermally eroded even directly above the plume stem makes thermal weakening of transform faults up to ∼1000 km away from the plume center unlikely.

An important aspect of the latest plate boundary reconfiguration is that it geometrically reestablished the original configuration of the linear unsegmented ridge that existed from just after continental breakup up until the change in opening direction near Anomaly 17 at ∼37 Ma (Fig. 1). This is demonstrated by Eulerian rotation of the present day Reykjanes Ridge axis following the North Atlantic closure poles of Smallwood and White (2002). Fig. 1A shows that the reconstructed Reykjanes Ridge axis closely matches the linear Anomaly 24–18 isochron trends (within 3°) despite the intervening breakup of the ridge into a stair-step pattern and a 30° rotation of the opening direction. This remarkable geometric congruence suggests a strong organizing mechanism acting on the plate boundary. The early plate boundary between the Bight FZ and Iceland appears to have formed in a linear configuration soon after Greenland–Eurasia continental breakup. Magnetic anomalies indicate a somewhat faster spreading rate than today (25–30 mm/yr full rate, Smallwood and White, 2002) but still slow spreading with enhanced melting due to elevated mantle temperature (White, 1997) and/or more fertile composition (Korenaga and Kelemen, 2000) possibly including elevated mantle water content (Nichols et al., 2002). Slow spreading induces a zone of sub-axial mantle upwelling that maintains a volume of mantle at the solidus from near the base of the crust to the damp solidus (melting regime). The deep low-viscosity damp melting interval within this zone is thus primed for a buoyant decompression melting convective instability (Raddick et al., 2002; Tackley and Stevenson, 1993). At slow spreading rates and under conditions that enhance melting and lower mantle viscosity, buoyant mantle upwelling is favored relative to purely plate-driven passive mantle upwelling (Bonatti et al., 2003; Braun et al., 2000; Choblet and Parmentier, 2001; Raddick et al., 2002; Scott and Stevenson, 1989; Sotin and Parmentier, 1989). The early-formed plate boundary would thus have been underlain by a linear zone of vigorous buoyant mantle upwelling, perhaps enhanced by the thermal structure of continental breakup itself (Mutter et al., 1988). Yet the typical expression of sub-axial buoyant mantle upwelling is a segmented crust, whether or not the ridge axis is offset. Magnetic and gravity maps (Fig. 1), however, show that the early plate boundary did not have offsets, FZs or other expressions of crustal segmentation so the axis was not underlain by multiple spatially stable buoyant mantle upwelling cells. It also seems unlikely that a single upwelling cell would have underlain the entire 1000-km-long axis, as buoyant mantle upwelling wavelengths are thought to scale with the thickness of the damp mantle melting interval between the wet and dry solidi (Braun et al., 2000; Choblet and Parmentier, 2001).

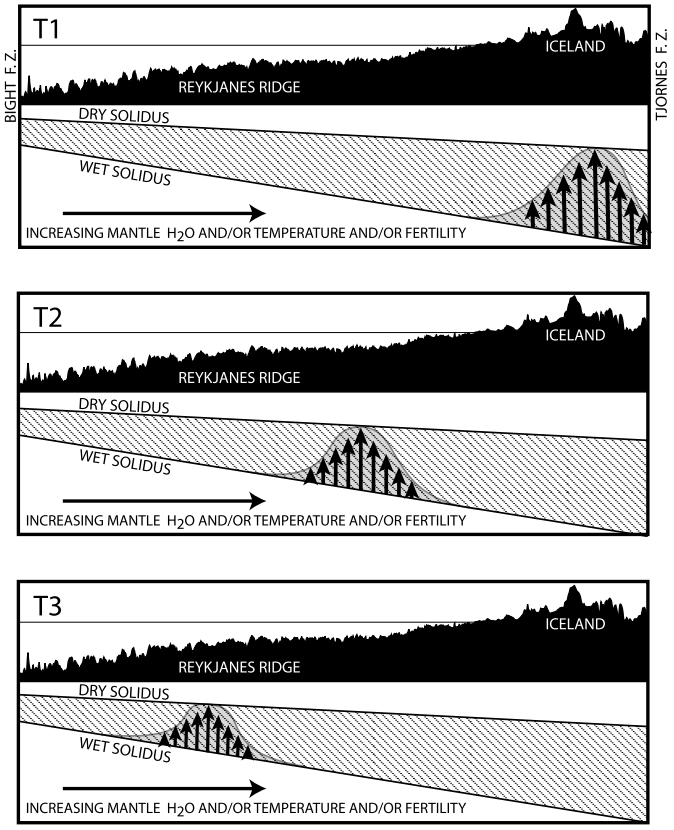

Fig. 5. Schematic vertical cross section depicting sub-axial propagating buoyant mantle upwelling along the Reykjanes Ridge. Panels T1–T3 depict sequential times showing the along-axis propagation of a cell of buoyant mantle upwelling indicated by the vertically pointing arrows and gray shaded area. The arrows indicate the component of buoyantly driven vertical advection in excess of that driven by background passive plate spreading. An area of "damp" melting between the wet and dry solidi (stippled area) is conducive to the formation of buoyant upwelling and is thicker near Iceland due to increased water content and perhaps increased temperature and mantle fertility there. Buoyant upwelling therefore initiates and is more vigorous beneath Iceland and propagates along the linear sub-axial melting regime of the Reykjanes Ridge. Propagation may also be promoted by the locally resistive density structure generated by buoyant upwelling itself, favoring continuation of the instability in adjacent areas. The linear sub-axial conduit is delimited by the Tjornes and Bight transform faults to the north and south respectively. Note that buoyant mantle flow is primarily vertical; it is only the temporal sequence of this flow that propagates horizontally along axis so that rapid horizontal mantle flow is not implied.

North Atlantic oceanic crustal thicknesses are observed to increase toward Iceland, indicating systematic variations in underlying mantle properties which may be due to temperature (White, 1997) and/or water content (Nichols et al., 2002) and/or composition (Korenaga and Kelemen, 2000). These effects lower mantle viscosity and deepen the solidus facilitating buoyant mantle upwelling. A plausible hypothesis is therefore that buoyant mantle upwelling instabilities initiate beneath Iceland, where mantle viscosity is lowest and the solidus deepest, and propagate southward beneath the long linear ridge along the sloping mantle solidus and viscosity gradient (Fig. 5). The density structure produced by buoyant upwelling tends to oppose the local continuation of buoyant upwelling, giving rise to its temporal variation (Scott and Stevenson, 1989; Sotin and Parmentier, 1989; Bonatti et al., 2003). Within the linear deep Reykjanes Ridge "damp" melting regime, local accumulation of residual buoyant mantle material may also help promote propagation of buoyant upwelling. On a long and linear ridge without offsets, local resistance to continued buoyant upwelling can simply cause continuation of the buoyant upwelling instability in adjacent along-axis areas. By propagating along axis, cells of buoyant mantle upwelling would thus not generate ridge-orthogonal segmentation discontinuities; instead they would form V-shaped crustal ridges and troughs (Crane, 1985) as observed in early-formed Reykjanes Ridge crust (Parnell-Turner et al., 2014) and following the elimination of transform faults (Hey et al., 2016). Propagation of buoyant mantle instabilities has been shown by geodynamic modeling to possibly operate in the subduction zone mantle wedge (Gerya and Yuen, 2003), but this effect has yet to be directly examined in numerical models of mid-ocean ridges.

When the change in opening direction occurred at about Anomaly 17 time (~37 Ma) the lithospheric plate boundary reacted nearly synchronously to the change in stresses and broke up into a new stair-step pattern aligned with the new opening direction and essentially centered over the previous plate boundary, as this would have been the weakest part of the lithosphere. However, a stair-step lithospheric plate boundary generates a more linear mantle upwelling zone at depth (Kuo and Forsyth, 1988) and in this case the pre-existing deep linear mantle upwelling zone may have simply persisted. Shallower mantle advection would have been more "passive" or "plate-driven" in form and closely followed the new plate boundary configuration (Phipps Morgan and Forsyth, 1988). Mantle viscosity layering may facilitate this partitioning of mantle upwelling. Mantle between the wet and dry solidi is thought to retain appreciable water, which significantly lowers its viscosity, whereas above the dry solidus mantle viscosity increases due to increased melting and extraction of water in melt (Braun et al., 2000; Hirth and Kohlstedt, 1996). Because of this viscosity layering, buoyant "active" mantle upwelling is thought to be favored in the low viscosity interval between the wet and dry solidi whereas plate-driven "passive" mantle upwelling predominates in the higher viscosity layer above the dry solidus (Bonatti et al., 2003; Braun et al., 2000; Choblet and Parmentier, 2001). Following the sudden change in opening direction and abrupt segmentation of the ridge axis the shallow stair-step plate-driven upwelling zone became misaligned with the deep linear buoyant mantle upwelling zone. The deep linear buoyant mantle upwelling zone persisted and guided the reassembly of the ridge back to its original configuration by promoting asymmetric spreading of individual offset segments (Fig. 6) and eventually the oblique linear alignment of the overall plate boundary zone. While the offset segments existed, shallower plate-driven advection within higher viscosity mantle would have guided melt delivery to the segmented axis resulting in segmented crust (Braun et al., 2000; Phipps Morgan and Forsyth, 1988). When orthogonal segment offsets became small enough (approximately the 15 km width of the plate boundary zone) the entire plate-driven and buoyant mantle upwelling geometry became aligned, linear and oblique. A long and linear plate boundary zone would induce corresponding two-dimensional passive mantle upwelling in the upper mantle, however the deeper propagating cells of buoyant upwelling would now be able to eliminate the previous nearly orthogonal crustal segmentation discontinuities, replacing them with V-shaped ridges and troughs—the expression of crustal segmentation when buoyant upwelling propagates.

As shown by MBAs (Fig. 4B), the orthogonally spreading segment south of the Bight FZ has a large (>20 mGal) bulls-eye gravity low but segments north of the Bight FZ display anomalies that progressively merge northward into a single linear and lengthening low with small along-axis variations. Gravity data north of our study area confirm only small amplitude (5–8 mGal) variations along the linear oblique axis (Searle et al., 1998). MBA gravity data and bathymetry from ridge flank areas show prominent FZ and NTD segmentation formed when ridge segments were spreading orthogonally (Fig. 4B) so that MBAs at that time would have formed large bulls-eye lows. The observed low amplitude MBA

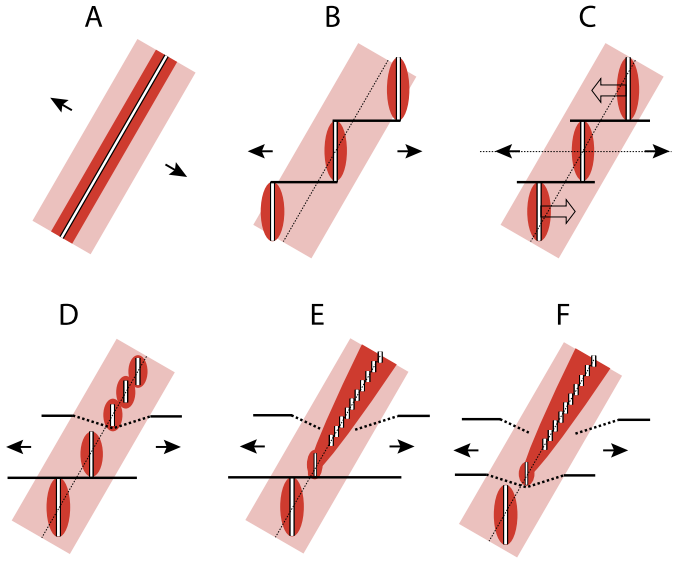

Fig. 6. Plan view kinematic model of the plate boundary reconfiguration. A) The original spreading center (double line) formed a long, linear, unsegmented axis from about anomaly 24 (~55 Ma) to anomaly 17 (~37 Ma). It spread in a NW–SE direction and produced an underlying linear mantle upwelling zone (deeper buoyant mantle upwelling indicated by pink color, shallower passive mantle upwelling by darker red). B) An abrupt change in opening direction to more E–W spreading at about anomaly 17 (~37 Ma) led to the mechanical breakup of the brittle lithosphere orthogonal to the new opening direction in a stair-step geometry, but roughly centered over the previous linear axis. The new segmented spreading axes induced their own plate-driven mantle upwelling patterns in the shallow mantle (dark red ovals) resulting in crustal segmentation but deeper buoyant mantle upwelling remained linear and centered over its original locus. C) After the change in opening direction at anomaly 17 no further significant changes in opening direction occurred. However, as the new spreading axes were not aligned with the underlying linear buoyant mantle upwelling zone the new segments migrated laterally to better align with the deep linear upwelling zone. D) Once ridge segment offsets approach the width of the plate boundary zone (~15 km) longer ridge segments fragment to smaller segments to better align to a linear plate boundary. Transform faults may also convert to migrating non-transform discontinuities as offsets decrease (dashed lines). E) Shallow plate-driven upwelling becomes two-dimensional as ridge offsets disappear and the overall plate boundary becomes linear, removing the previous crustal segmentation. F) The north to south progression of elimination of segmentation and formation of a linear oblique axis is driven by the southward propagation of buoyant mantle upwelling cells that result in V-shaped crustal ridges. In the pulsing plume model there is no linear low-viscosity deep "damp" melting interval (pink area) as the entire melting regime is within the high-viscosity dehydration layer. Therefore when the change in opening direction occurs and the plate boundary becomes segmented (B) the entire melting regime is embedded in the high viscosity dehydration layer and mirrors the segmented plate boundary configuration, which should remain stable given the proposed resistance of this strong layer to mantle plume flow and thermal erosion in the pulsing plume model.

gravity variations along the oblique axis today thus support the interpretation that large bulls-eye lows corresponding to the previous segmented crust were replaced by longer wavelength MBA variations that now span the previous segments. The wavelength of the propagating buoyant mantle upwelling cells can be estimated from the along-axis length of shallow crust that forms the V-shaped ridges. Based on the identification of Searle et al. (1998) the current axial V-shaped ridge with a southern tip near 59.5°N extends for ~250 km along axis, which is significantly longer than typical Reykjanes Ridge flank FZ spacings of ~50 to 100 km. As these V-shaped gravity and bathymetry ridges and troughs now intersect the axis at acute angles their on-axis expression is spread out over a longer length than when they were nearly orthogonally oriented to the axis giving the impression of an unsegmented axis. However, the V-shaped ridges and troughs are in fact seismically estimated to have crustal thickness variations of about 2–3 km (White et al., 1995), indicating significant crustal segmentation.

We hypothesize that buoyant mantle upwelling cells originate as episodic instabilities (Scott and Stevenson, 1989; Sotin and Parmentier, 1989) beneath Iceland where mantle water content is most elevated (Nichols et al., 2002) and where temperature and/or mantle fertility may also be highest. Gradients in these mantle properties southward may promote gravitationally driven propagation of the instabilities due to changes in buoyancy (associated with changes in composition and mantle volatile content) and due to the associated sloping solidi (see Fig. 5). The instabilities may also propagate monotonically southward due to the local density structure that they generate as inherently buoyant residual mantle material accumulates, which tends to resist continuation of local buoyant upwelling. Buoyant upwelling may therefore continue in an adjacent location along-axis where excess residual mantle has not yet accumulated. The major long-lived offsets in the plate boundary at the Bight and Tjornes transform faults delimit the linear axis along which propagation occurs. Between the episodes of buoyant mantle upwelling sub-axial mantle flow is plate-driven "passive" in form (Scott and Stevenson, 1989). With time, the resistive thermal and compositional density structure generated by buoyant upwelling is relieved by cooling and plate spreading and the process can repeat. Since buoyant mantle upwelling involves faster rates than the intervening stages of passive-like upwelling (Plank and Langmuir, 1992), it generates more melt and is subject to less cooling. As the shape of the buoyant melting regime and the streamlines of mantle flow are more focused than in the broad triangular melting regimes of passive upwelling (Plank and Langmuir, 1992), melts have geochemical signatures typically interpreted as hotter temperatures and greater extents of melting (Braun et al., 2000), yet greater melting is actually produced by a larger and more focused flux of mantle through the buoyant melting regime, not greater temperature. These geochemical signatures have in fact been identified in axial rock samples, but interpreted as thermal variations from a "pulsing" mantle plume (Jones et al., 2014). The varying melt production associated with buoyant upwelling and intervening passive-like upwelling (Scott and Stevenson, 1989) can therefore explain the V-shaped ridges and troughs (Fig. 7C) without mantle temperature variations. The additional crustal thickness of the V-shaped ridges relative to the troughs is only about 2 km of the typical 10–11 km total crustal thickness of unsegmented crust implying that this reflects the additional fraction of melting associated with the passage of a buoyant upwelling cell relative to intervening passive spreading. Dynamic and isostatic forces associated with episodes of buoyant upwelling may also generate corresponding regional flexural seafloor uplift affecting North Atlantic sedimentation patterns, currently thought in some models to be due to a pulsing mantle plume and associated thermal uplift (e.g., Poore et al., 2011).

Seismic anisotropy measurements provide further observational support for the role of vigorous buoyant mantle upwelling beneath the Reykjanes Ridge. An unusual but prominent aspect of the North Atlantic basin surrounding the Reykjanes Ridge is strong vertically polarized seismic anisotropy in the upper mantle (Gaherty, 2001). Seismic anisotropy caused by seafloor spreading is explained by alignment of the fast a-axes in olivine crystals due to mantle flow and shearing. In the North Atlantic the unusual degree of vertical anisotropy has been attributed to especially strong sub-axial buoyant mantle upwelling beneath the Reykjanes Ridge that imparts a vertical flow structure to olivine crystals in ridge flank mantle (Gaherty, 2001). In contrast, the pulsing plume model cannot account for vertical seismic anisotropy as it predicts only horizontal anisotropy perpendicular to the axis due to the high viscosity rheological boundary that permits only plate-driven mantle corner flow above the solidus (Fig. 7A) and horizontal radial plume spreading beneath the depth of significant seismic anisotropy (>150 km).

More recent analyses of seismic anisotropy in the North Atlantic basin also indicate that the anisotropy patterns can be explained by a component of along-axis flow (Delorey et al., 2007).

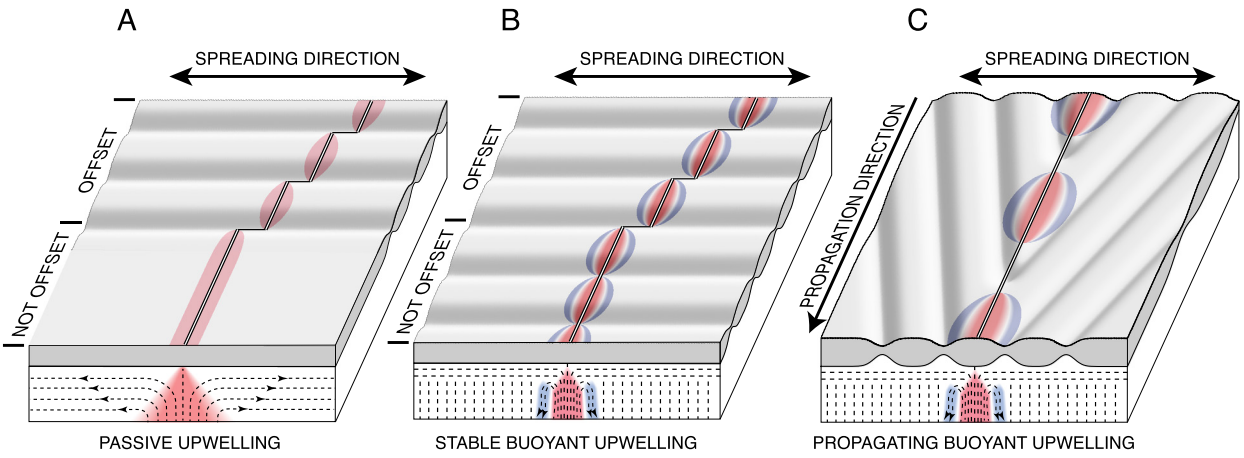

Fig. 7. Crustal segmentation and mantle upwelling. Colored ovals depict the surface projection of mantle upwelling cells with red indicating upward advection and blue downward flow. Frontal facades depict a vertical section with dashed lines indicating mantle flow in colored areas and frozen-in fabric in blank areas. Along the ridge axis (fine double line) the upwelling cells produce thicker crust near their centers and thinner crust near their ends as depicted in the crustal layer (gray). Not shown are temporal variations in buoyant upwelling (Scott and Stevenson, 1989) leading to second-order crustal thickness variations in the spreading direction (Bonatti et al., 2003). (A) Plate-driven or passive mantle upwelling produces crustal segmentation only at ridge axis offsets and can only generate horizontal flow fabric and horizontal seismic anisotropy on ridge flanks unlike the pronounced vertical anisotropy observed on the Reykjanes Ridge flanks. (B) Spatially stable buoyant mantle upwelling cells (colored ovals) produce crustal segmentation whether or not the ridge segments are offset by transform faults (thin solid lines) (Tucholke et al., 1997). (C) On a linear axis underlain by gradients in mantle properties (see Fig. 5), buoyant upwelling cells can propagate systematically along axis producing crustal V-shaped ridges and troughs whose geometry is a function of the propagation rate of the instability and spreading rate. Especially strong buoyant upwelling on the Reykjanes Ridge results in pronounced vertical seismic anisotropy (Gaherty, 2001).

Axially propagating buoyant instabilities may generate a transient component of shear fabric along axis as mantle material diverges from the center of the propagating instability. Thus some axis-parallel anisotropy is predicted by axially propagating buoyant upwelling instabilities. However, such flow is precluded in the pulsing plume model due to the high viscosity "rheological boundary" that permits only plate-driven corner flow perpendicular to the ridge (Ito, 2001). Thus the seismic anisotropy measurements of shallow (<150 km) vertical and/or along-axis structure are inconsistent with pulsing plume models but are predicted by propagating buoyant upwelling instabilities. Delorey et al. (2007) also discount effects related to high melt content in shaping the seismic anisotropy differently from shear-related mantle flow.

Along-axis propagation of buoyant mantle upwelling does not imply that mantle material is moving along axis at the steady-state rate of propagation (Figs. 5 and 7C). Although the buoyant upwelling instabilities move along axis at the rate indicated by the geometry of the V-shaped ridges (roughly 10 times the spreading rate), mantle material flow in the buoyant cells is primarily up and down laterally across the axis (Fig. 7C) and need only be at an upwelling rate necessary to produce the additional crustal thickness of the V-shaped ridges relative to the troughs separating them (about 2 km). A small component of along axis flow may be generated by the transient passage of the upwelling instability, but most shear flow fabric frozen into the ridge flanks is predicted to be vertical. This property of propagating buoyant mantle upwelling removes the need for high radial mantle flow velocities, even higher plume stem upwelling rates, thermal anomalies embedded in plume flow, and the rheological dehydration boundary required to laterally deflect plume material beneath the solidus and prevent unrealistic crustal thicknesses inherent in pulsing plume models (Ito, 2001; Jones et al., 2014, 2002; Vogt, 1971).

Another feature of our model is that it explains regional changes in crustal thickness associated with transitions between unsegmented and segmented crust (e.g., White, 1997) without changes in regional mantle temperature. Changes in regional average crustal thickness can be directly explained by changes in ridge segmentation itself. This occurs because upwelling beneath segmented spreading centers reaches a maximum near the segment center and decreases markedly toward segment ends (to zero for large offsets) (Kuo and Forsyth, 1988; Phipps Morgan and Forsyth, 1988). At large-offset slow spreading centers crustal thinning toward segment ends may occur over 40 km (Whitmarsh and Calvert, 1986). Typical ridge lengths on the Reykjanes Ridge during its segmented stage were only about 50 km, thus essentially the entire plate boundary was affected by this segmentation effect relative to the unsegmented axis before and after this stage. Thus changes from segmented spreading to unsegmented spreading can produce significant overall changes in crustal thicknesses that are a consequence of segmentation and the geometry of upwelling it induces, not mantle temperature (Martinez et al., 2002). The MBA map (Fig. 4B) shows that north of the Bight FZ the gravity low widens continually northward, unlike the typical bulls-eye patterns at slow-spreading ridges, indicating a progressive widening of thicker crust corresponding to the progressively older elimination of segmentation. Segmentation control on mantle upwelling, melting and crustal thickness provides an alternative explanation for regional crustal thickness changes associated with the segmentation of the Reykjanes Ridge and previously attributed to thermal effects of regional plume flux advances and withdrawals (Jones, 2003; Parnell-Turner et al., 2014; White, 1997).

5. Summary and conclusions

The Reykjanes Ridge underwent three main stages in its evolution (White, 1997): 1) early orthogonal spreading on a long linear axis without FZs or NTDs; 2) orthogonal spreading on stair-step offset ridge segments following an abrupt change in spreading direction forming FZs and NTDs; 3) a progressive north-to-south elimination of ridge offsets and FZs and NTDs reforming a long, linear but now obliquely spreading axis with flanking V-shaped ridges and troughs. We have carried out a geophysical survey of the southern end of the Reykjanes Ridge and flanks in order to investigate the geologic mechanisms of plate boundary reconfiguration and associated changes in crustal accretion in the latest stage (3) of its evolution. The data support a new model for the kinematic evolution of the Reykjanes Ridge and the geodynamic processes involved.

Magnetic anomaly data show that orthogonally spreading and offset ridge segments first migrate laterally to reduce segment offsets. Longer segments then break up into smaller segments to better align to a linear oblique axis. The process culminates with a linear but now oblique plate boundary zone formed by en echelon axial volcanic ridges that have retained their nearly spreading-orthogonal geometry throughout the reconfiguration. Plate boundary reconstructions show that the linear Reykjanes Ridge axis today is within about 3° of the orientation and directly over the position of the initial unsegmented spreading center despite a ∼30° change in opening direction and intervening fragmentation of the axis. This geometric alignment suggests that the deep linear buoyant mantle upwelling zone generated by the initial spreading center persisted even after the axis became segmented and controlled its subsequent reconfiguration back to its original geometry. We propose that sub-axial cells of buoyant mantle upwelling initiate near Iceland and propagate southward driven by gradients in mantle properties (water content/temperature/composition). MBA patterns indicate that propagation of buoyant mantle upwelling replaces the previous orthogonal crustal segmentation forming bullseye lows with more uniform long wavelength advection. Cells of propagating sub-axial buoyant mantle upwelling also generate locally increased crustal thickness and explain the V-shaped ridges flanking the linear Reykjanes Ridge. By changing the pattern of mantle advection, removal of segmentation in itself increases melt production and crustal thickness without changes in mantle temperature. Thus crustal features and tectonic reconfigurations of the Reykjanes Ridge are not necessarily indicators of mantle plume flow or temperature variations in the mantle. Buoyantly upwelling mantle material flows primarily vertically and is then frozen into ridge flank lithosphere with only the temporal locus of the instabilities moving rapidly along-axis. Thus extremely high mantle upwelling and lateral flow velocities are not implied as in "pulsing plume" models and there is no need to invoke an Iceland-specific mantle dehydration layer to deflect rapidly upwelling mantle beneath Iceland and avoid unrealistic crustal thicknesses.

There is clearly a mantle melting anomaly in the North Atlantic centered near Iceland and our data and model do not directly address the nature of this anomaly or the existence of a mantle plume. However, the new geophysical data indicate that the tectonic reorganizations of the Reykjanes Ridge and its flanking V-shaped ridges can be better explained by kinematic and plate boundary processes rather than deep mantle plume flow.

Author contributions

FM wrote the initial draft of the paper and developed the propagating buoyant mantle upwelling model. RH is principal investigator and conceived the Reykjanes Ridge tectonic reconfiguration project. Both authors collaborated closely on the final formulation of the paper.

Competing financial interests

The authors declare that they have no competing financial interests.

Acknowledgements

Underway geophysical data are available at http://www.rvdata.us/catalog/MGL1309. This work was supported by NSF grant OCE-1154071. We thank the Captain and crew of R/V Marcus G. Langseth and the science party and Brian Taylor for comments. We also thank two anonymous reviewers for their constructive evaluations and the government of Iceland for permission to work in their waters. HIGP contribution #2227, SOEST contribution #9388.

References

Benediktsdóttir, Á., Hey, R., Martinez, F., Höskuldsson, Á., 2016. A new kinematic model of the Mid-Atlantic Ridge between 55°55′N and the Bight transform fault for the past 6 Ma. J. Geophys. Res., Solid Earth 121, 455–468.

Bonatti, E., Ligi, M., Brunelli, D., Cipriani, A., Fabretti, P., Ferrante, V., Gasperini, L., Ottolini, L., 2003. Mantle thermal pulses below the Mid-Atlantic Ridge and temporal variations in the formation of oceanic lithosphere. Nature 423, 499–505.

Braun, M.G., Hirth, G., Parmentier, E.M., 2000. The effects of deep damp melting on mantle flow and melt generation beneath mid-ocean ridges. Earth Planet. Sci. Lett. 176, 339–356.

Caress, D.W., Chayes, D.N., 2008. MB-System. http://www.ldeo.columbia.edu/res/pi/MB-System/.

Choblet, G., Parmentier, E.M., 2001. Mantle upwelling and melting beneath slow spreading centers: effects of variable rheology and melt productivity. Earth Planet. Sci. Lett. 184, 589–604.

Crane, K., 1985. The spacing of rift axis highs: dependence upon diapiric processes in the underlying asthenosphere? Earth Planet. Sci. Lett. 72, 405–414.

Delorey, A.A., Dunn, R.A., Gaherty, J.B., 2007. Surface wave tomography of the upper mantle beneath the Reykjanes Ridge with implications for ridge–hot spot interaction. J. Geophys. Res., Solid Earth 112, B08313.

Forsyth, D.W., 1992. Geophysical constraints on mantle flow and melt generation beneath mid-ocean ridges. In: Phipps-Morgan, J., Blackman, D.K., Sinton, J.M. (Eds.), Mantle Flow and Melt Generation at Mid-Ocean Ridgess. American Geophysical Union, Washington, D.C., pp. 1–65.

Gaherty, J.B., 2001. Seismic evidence for hotspot-induced buoyant flow beneath the Reykjanes Ridge. Science 293, 1645–1647.

Gerya, T.V., Yuen, D.A., 2003. Rayleigh–Taylor instabilities from hydration and melting propel 'cold plumes' at subduction zones. Earth Planet. Sci. Lett. 212, 47–62.

Goodliffe, A.M., Taylor, B., Martinez, F., Hey, R., Maeda, K., Ohono, K., 1997. Synchronous reorientation of the Woodlark Basin spreading center. Earth Planet. Sci. Lett. 146, 233–242.

Hey, R.N., 1977. A new class of "pseudofaults" and their bearing on plate tectonics: a propagating rift model. Earth Planet. Sci. Lett. 37, 321–325.

Hey, R.N., Duennebier, F.K., Morgan, W.J., 1980. Propagating rifts on mid-ocean ridges. J. Geophys. Res., Solid Earth 85, 3647–3658.

Hey, R., Martinez, F., Höskuldsson, Á., Benediktsdóttir, Á., 2010. Propagating rift model for the V-shaped ridges south of Iceland. Geochem. Geophys. Geosyst. 11, Q03011.

Hey, R., Martinez, F., Höskuldsson, Á., Eason, D.E., Sleeper, J., Thordarson, S., Benediktsdóttir, Á., Merkuryev, S., 2016. Multibeam investigation of the active North Atlantic plate boundary reorganization tip. Earth Planet. Sci. Lett. 435, 115–123.

Hirth, G., Kohlstedt, D.L., 1996. Water in the oceanic upper mantle: implications for rheology, melt extraction and the evolution of the lithosphere. Earth Planet. Sci. Lett. 144, 93–108.

Ito, G., 2001. Reykjanes 'V'-shaped ridges originating from a pulsing and dehydrating mantle plume. Nature 411, 681–684.

Jones, S.M., 2003. Test of a ridge–plume interaction model using oceanic crustal structure around Iceland. Earth Planet. Sci. Lett. 208, 205–218.

Jones, S.M., Murton, B.J., Fitton, J.G., White, N.J., Maclennan, J., Walters, R.L., 2014. A joint geochemical–geophysical record of time-dependent mantle convection south of Iceland. Earth Planet. Sci. Lett. 386, 86–97.

Jones, S.M., White, N., Maclennan, J., 2002. V-shaped ridges around Iceland: implications for spatial and temporal patterns of mantle convection. Geochem. Geophys. Geosyst. 3. http://dx.doi.org/10.1029/2002GC000361.

Korenaga, J., Kelemen, P.B., 2000. Major element heterogeneity in the mantle source of the North Atlantic igneous province. Earth Planet. Sci. Lett. 184, 251–268.

Kuo, B.-Y., Forsyth, D.W., 1988. Gravity anomalies of the ridge–transform system in the south Atlantic between 31 and 34.5°S: upwelling centers and variations in crustal thickness. Mar. Geophys. Res. 10, 205–232.

Lee, S.-M., Searle, R.C., 2000. Crustal magnetization of the Reykjanes Ridge and implications for its along-axis variability and the formation of axial volcanic ridges. J. Geophys. Res., Solid Earth 105, 5907–5930.

Luis, J.F., 2007. Mirone: a multi-purpose tool for exploring grid data. Comput. Geosci. 33, 31–41.

Macdonald, K.C., 1982. Mid-ocean ridges: fine scale tectonic, volcanic and hydrothermal processes within the plate boundary zone. Annu. Rev. Earth Planet. Sci. 10, 155–190.

Macnab, R., Verhoef, J., Roest, W., Arkani-Hamed, J., 1995. New database documents the magnetic character of the Arctic and North Atlantic. Eos 76. 449 and 458.

Martinez, F., Karsten, J., Milman, M., Klein, E., 2002. Segmentation control on crustal accretion: insights from the Chile Ridge. AGU Fall Meeting Suppl. 83, Abstract T72C-06.

Merkouriev, S., DeMets, C., 2014. High-resolution Neogene reconstructions of Eurasia–North America plate motion. Geophys. J. Int. http://dx.doi.org/10.1093/gji/ggu142.

Morgan, W.J., 1971. Convection plumes in the lower mantle. Nature 230, 43–44.

Mutter, J.C., Buck, W.R., Zehnder, C.M., 1988. Convective partial melting, 1: a model for the formation of thick basaltic sequences during the initiation of spreading. J. Geophys. Res., Solid Earth 93, 1031–1048.

Nichols, A.R.L., Carroll, M.R., Höskuldsson, Á., 2002. Is the Iceland hot spot also wet? Evidence from the water contents of undegassed submarine and subglacial pillow basalts. Earth Planet. Sci. Lett. 202, 77–87.
Okino, K., Kasuga, S., Ohara, Y., 1998. A new scenario of the Parece Vela Basin genesis. Mar. Geophys. Res. 20, 21–40.
Parker, R.L., 1972. The rapid calculation of potential anomalies. Geophys. J. R. Astron. Soc. 31, 447–455.
Parnell-Turner, R., White, N., Henstock, T., Murton, B., Maclennan, J., Jones, S.M., 2014. A continuous 55-million-year record of transient mantle plume activity beneath Iceland. Nat. Geosci. 7, 914–919.
Parson, L.M., Murton, B.J., Searle, R.C., Booth, D., Evans, J., Field, P., Keeton, J., Laughton, A., McAllister, E., Millard, N., Redbourne, L., Rouse, I., Shor, A., Smith, D., Spencer, S., Summerhayes, C., Walker, C., 1993. En echelon volcanic ridges at the Reykjanes Ridge: a life cycle of volcanism and tectonism. Earth Planet. Sci. Lett. 117, 73–87.
Phipps Morgan, J., Forsyth, D.W., 1988. Three-dimensional flow and temperature perturbations due to a transform offset: effects on oceanic crustal and upper mantle structure. J. Geophys. Res., Solid Earth 93, 2955–2966.
Plank, T., Langmuir, C.H., 1992. Effects of the melting regime on the composition of the oceanic crust. J. Geophys. Res., Solid Earth 97, 19749–19770.
Poore, H., White, N., Maclennan, J., 2011. Ocean circulation and mantle melting controlled by radial flow of hot pulses in the Iceland plume. Nat. Geosci. 4, 558–561.
Raddick, M.J., Parmentier, E.M., Scheirer, D.S., 2002. Buoyant decompression melting: a possible mechanism for intraplate volcanism. J. Geophys. Res. 107 (B10). http://dx.doi.org/10.1029/2001JB000617.
Reid, I., Jackson, H.R., 1981. Oceanic spreading rate and crustal thickness. Mar. Geophys. Res. 5, 165–172.
Sandwell, D.T., Müller, R.D., Smith, W.H.F., Garcia, E., Francis, R., 2014. New global marine gravity model from CryoSat-2 and Jason-1 reveals buried tectonic structure. Science 346, 65–67.
Scott, D.R., Stevenson, D.J., 1989. A self-consistent model of melting, magma migration and buoyancy-driven circulation beneath mid-ocean ridges. J. Geophys. Res., Solid Earth 94, 2973–2988.
Searle, R.C., Keeton, J.A., Owens, R.B., White, R.S., Mecklenburgh, R., Parsons, B., Lee, S.M., 1998. The Reykjanes Ridge: structure and tectonics of a hot-spot-influenced, slow-spreading ridge, from multibeam bathymetry, gravity and magnetic investigations. Earth Planet. Sci. Lett. 160, 463–478.
Smallwood, J.R., White, R.S., 2002. Ridge–plume interaction in the North Atlantic and its influence on continental breakup and seafloor spreading. Geol. Soc. (Lond.) Spec. Publ., vol. 197. Geological Society, London, pp. 15–37.
Sotin, C., Parmentier, E.M., 1989. Dynamical consequences of compositional and thermal density stratification beneath spreading centers. Geophys. Res. Lett. 16, 835–838.
Tackley, P.J., Stevenson, D.J., 1993. A mechanism for spontaneous self-perpetuating volcanism on the terrestrial planets. In: Stone, D.B., Runcorn, S.K. (Eds.), Flow and Creep in the Solar System: Observations, Modeling and Theory. Kluwer Academic Publishers, The Netherlands, pp. 307–321.
Tucholke, B.E., Lin, J., Kleinrock, M.C., Tivey, M.A., Reed, T.B., Goff, J., Jaroslow, G.E., 1997. Segmentation and crustal structure of the western Mid-Atlantic Ridge flank, 25°25′–27°10′N and 0–29 m.y. J. Geophys. Res., Solid Earth 102 (10), 203–210. 223.
Vogt, P.R., 1971. Asthenosphere motion recorded by the ocean floor south of Iceland. Earth Planet. Sci. Lett. 13, 153–160.
Vogt, P.R., Avery, O.E., 1974. Detailed magnetic surveys in the northeast Atlantic and Labrador Sea. J. Geophys. Res., Solid Earth 79, 363–389.
Vogt, P.R., Johnson, G.L., 1975. Transform faults and longitudinal flow below the Midoceanic Ridge. J. Geophys. Res. 80, 1399–1428.
Wessel, P., Smith, W.H.F., Scharroo, R., Luis, J., Wobbe, F., 2013. Generic mapping tools: improved version released. Eos 94, 409–410.
White, R.S., 1997. Rift–plume interaction in the North Atlantic. Philos. Trans. R. Soc., Math. Phys. Eng. Sci. 355, 319–339.
White, R.S., Bown, J.W., Smallwood, J.R., 1995. The temperature of the Iceland plume and origin of outward-propagating V-shaped ridges. J. Geol. Soc. 152, 1039–1045.
Whitmarsh, R.B., Calvert, A.J., 1986. Crustal structure of Atlantic fracture zones, I: the Charlie–Gibbs fracture zone. Geophys. J. Int. 85, 107–138.
Wright, J.D., Miller, K.G., 1996. Control of North Atlantic Deep Water circulation by the Greenland–Scotland Ridge. Paleoceanography 11, 157–170.